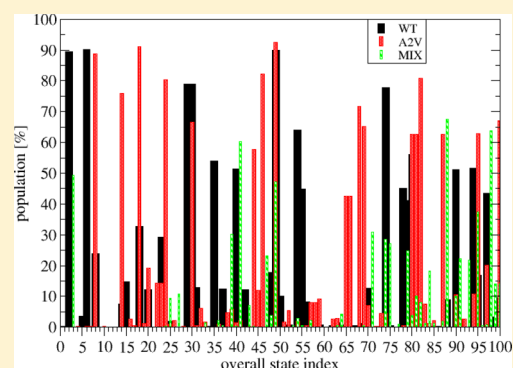


Impact of the A2V Mutation on the Heterozygous and Homozygous A β 1–40 Dimer Structures from Atomistic SimulationsPhuong H. Nguyen,[†] Fabio Sterpone,[†] Josep M. Campanera,[‡] Jessica Nasica-Labouze,[†] and Philippe Derreumaux^{*,†}[†]Laboratoire de Biochimie Théorique, UPR 9080 CNRS, Université Paris Diderot, Sorbonne Paris Cité, IBPC, 13 Rue Pierre et Marie Curie, 75005 Paris, France[‡]Departament de Físicoquímica, Facultat de Farmàcia, Universitat de Barcelona, 08028 Barcelona, Catalonia, Spain

ABSTRACT: The A2V mutation was reported to protect from Alzheimer's disease in its heterozygous form and cause an early Alzheimer's disease type dementia in its homozygous form. Experiments showed that the aggregation rate follows the order A2V > WT (wild-type) > A2V-WT. To understand the impact of this mutation, we carried out replica exchange molecular dynamics simulations of A β 1–40 WT-A2V and A2V-A2V dimers and compared to the WT dimer. Our atomistic simulations reveal that the mean secondary structure remains constant, but there are substantial differences in the intramolecular and intermolecular conformations upon single and double A2V mutation. Upon single mutation, the intrinsic disorder is reduced, the intermolecular potential energies are reduced, the population of intramolecular three-stranded β -sheets is increased, and the number of all α dimer topologies is decreased. Taken together, these results offer an explanation for the reduced aggregation rate of the A β 1–40 A2V-WT peptides and the protective effect of A2V in heterozygotes.

KEYWORDS: Amyloid, atomistic simulations, A β peptide, dimers, A2V mutation



The wild-type (WT) A β 1–40 peptide of sequence DAEFRHDSGYEVHHQKLVFFAEDVGSNKGAIIGLMVGGVV with the hydrophobic patches L17-A21 and A30-V40 and the hydrophilic patches D1-K16 and E22-G29 is the major constituent of extracellular amyloid plaques in the human brain.¹ It is known that WT A β dimers are sufficient to induce cognitive deficits² and dimers stabilized by an intermolecular disulfide bridge via a mutation S8C cause early deficits in synaptic plasticity, learning and memory.³ Preventing dimerization by small molecules is thus considered as one therapeutic target to cure Alzheimer's disease (AD).^{4–6}

In 2009 Di Fede et al. described a new amyloid precursor protein mutation consisting of a C-to-T transition at position 673 that causes an alanine-to-valine substitution at position 2 of A β peptide in an Italian family.⁷ While the A2V mutation increases A β 1–40 and A β 1–42 production, homozygous carriers inherited from both parents present early onset AD, but heterozygous carriers do not develop AD. Using neuroblastoma SH-SY5Y cells and MTT, A β 1–42 A2V was found more toxic than A β 1–42 WT, and the mixture was significantly less toxic than either peptide alone.⁷

The experimental sigmoidal aggregation kinetics is described qualitatively by means of primary and secondary (fragmentation or lateral process involving fibril surface) nucleation processes.^{8,9} The aggregation kinetics of the A β 1–40 WT and A2V peptides and the equimolar mixture (A β 1–40 MIX) was studied by laser light scattering and the time of aggregate formation of A β 1–40 MIX was higher (8.3 h) than the time to

aggregate for either A β 1–40 A2V (1.3 h) or A β 1–40 WT (5.8 h).⁷ Using size exclusion chromatography, the oligomer size distribution in A β 1–40 MIX was lowest at time 0 and after 24 h, and the A β 1–40 MIX aggregates were less stable than those generated by either A β 1–40 WT or A β 1–40 A2V after dilution with buffer.⁷ Using ion mobility mass spectrometry (IM-MS), A2V caused A β 1–40 to aggregate similarly to A β 1–42 WT with the formation of dimers, tetramers, hexamers and dodecamers, while the WT/A2V mixture inhibited formation of hexamers and dodecamers.¹⁰ A slower kinetics of A β 1–42 MIX with respect to WT was also hypothesized to be due to the difficulty of the two peptides to form stable intermolecular interactions.¹¹ Overall, we lack the structures of the dimers and small oligomers to comprehend the difference in the aggregation kinetics of A β peptides upon single and double A2V mutation.

Since A β 1–40 is 10 times more prevalent than A β 1–42 in plaques and dimers are key players in AD etiology, we have determined the conformations of A β 1–40 A2V and WT-A2V dimers by all-atom REMD simulations with the all-atom CHARMM22* force field. CHARMM22* is one of the best force fields for folded proteins^{12,13} and leads to results consistent with experimental data on the A β 1–28 monomer¹⁴ alone or interacting with the compound NQTp.^{4,15} By

Received: February 22, 2016

Accepted: March 23, 2016

Published: March 23, 2016

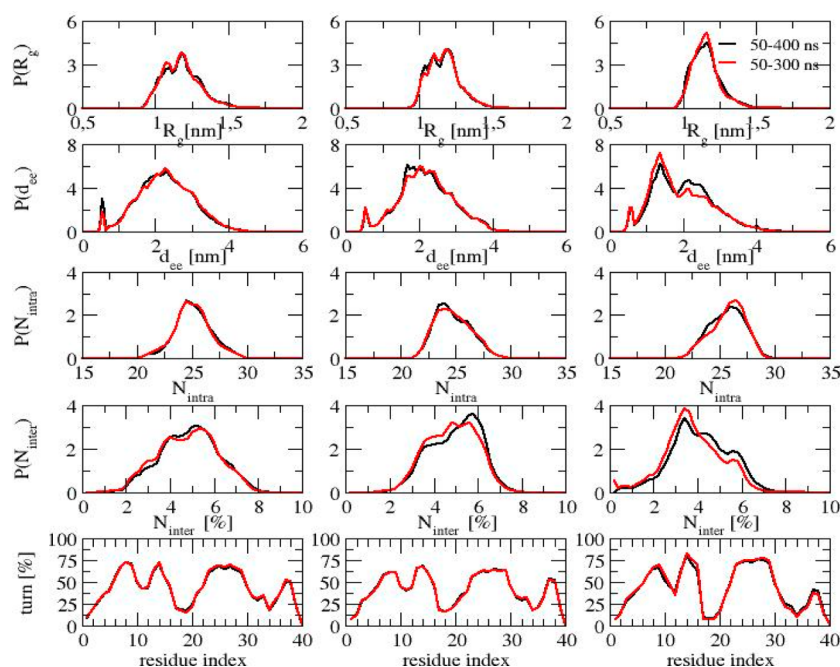


Figure 1. Convergence of the REMD simulations. Distributions of various quantities including the radius of gyration (R_g), the end-to-end distance (d_{ee}), the total number of intra (N_{intra}), interpeptide contacts (N_{inter}), and the turn populations (turn) of the WT (left panels), A2V (middle panels), and MIX (right panels) dimers. Shown are results obtained from 50–300 ns (black) and 50–400 ns (red) of the REMD trajectory at 315 K.

comparing with the REMD results on β 1–40 WT dimer,¹⁶ we provide for the first time a detailed description of the change induced by the A2V mutation in the hetero- and homozygous forms of β 1–40 dimer. Note that the dimers of β 1–40/1–42 WT peptides and their disease-causing mutants in the N-terminus (H6R, D7N), CHC (A21G) and loop region (E22G/K, D23N) were subject to simulations with various protein and water models,^{1,17–21} but the effect of A2V has only been studied by computer means on the β 1–28¹⁴ and β 1–42 monomers.²²

RESULTS AND DISCUSSION

Convergence. To assess convergence of the simulations at 315 K, near the physiological temperature, we calculated the distributions of several metrics calculated over the time intervals of 50–300 ns and 50–400 ns. The metrics include the radius of gyration, the end-to-end distance between the C_α atoms of the first and last residues of each peptide, the number of intra- and intermolecular SC–SC contacts and the percentage of each amino acid to adopt a turn.

As it can be seen in Figure 1, the results obtained using the data from 50–300 ns and 50–400 ns trajectories are virtually identical indicating that the three systems have reached equilibrium. The R_g distributions in Figure 1a do not show significant variations with time and have an average value of 1.17 ± 0.1 nm in WT and A2V and 1.14 ± 0.1 nm in MIX. The mean end-to-end distance is 2.22 ± 0.1 nm in WT, 2.17 ± 0.1 nm in A2V and 1.98 ± 0.2 nm in MIX, indicating that the conformations are less extended in the heterozygous form (Figure 1b). In WT, there are 95%, 61%, and 15% of the conformations with end-to-end distances >1 , >2 , and >3 nm, respectively. The values are 95%, 57% and 13% in A2V dimers vs 92%, 47% and 10% in MIX dimers. The distributions of the SC–SC contacts in Figure 1 are broad and show that MIX displays more intramolecular contacts than the peptide WT and A2V alone, with mean Q values of 28%, 25%, and 23%,

respectively, at the expense of a reduced number of intermolecular contacts, with mean Q values of 3% vs 5% in WT and 7% in A2V. The turn profiles in WT and A2V are nearly identical (Figures 1 and 2), and differ from the turn profile in MIX with variations of $\pm 10\%$ at specific positions.

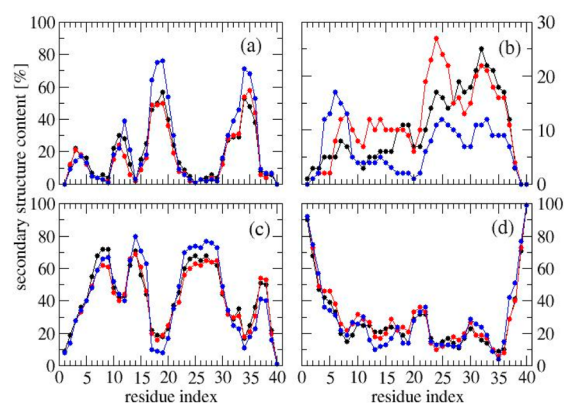


Figure 2. Secondary structure propensities. Populations (in %) of β -strand (a), α -helix (b), turn (c), and coil (d) various secondary structures along the residues averaged over two chains of the WT (black), A2V (red), and MIX (blue). Shown are results obtained from 50–400 ns of the REMD trajectory at 315 K.

As another proof of the convergence of simulations, we used two independent time windows (150–275 ns and 275–400 ns). All distributions and turn profiles between the distinct time windows superpose very well, but are not strictly identical, indicating that convergence of the equilibrium ensembles requires a time scale of 400 ns.

In what follows, analysis was performed on the conformations at 315 K within the time interval of 50–400 ns. Statistical deviations were estimated by calculating block averages over different the time intervals of 50–225 and 225–400 ns.

Secondary Structure. The mean and standard deviation of secondary structures averaged over the two chains are reported in Table 1. Averaged over all residues, the A2V mutation does

Table 1. Secondary Structures^a

SS [%]	WT	A2V	MIX
β	18.5 (3.3)	16.8 (2.8)	21.6 (4.2)
α	10.0 (2.7)	11.7 (3.2)	6.9 (3.3)
turn	43.2 (3.7)	41.3 (3.3)	42.9 (4.9)
coil	28.2 (3.1)	30.3 (3.2)	28.6 (4.6)

^aMean and standard deviation (in parentheses) of SSs in %. The standard deviations are calculated using block average analysis. Shown are results obtained from 50–400 ns of the REMD trajectory at 315 K.

not change the coil and turn populations with mean values of $29 \pm 3.4\%$ and $42 \pm 3.7\%$, respectively. The mutations impact, however, the (β -strand, α -helix) contents with a shift from (16.8, 11.7%) in A2V to (21.7, 6.7%) in MIX and (18.7, 10.0%) in WT. Figure 2 shows the 2D structure propensities along the sequence in the three systems. The β and turn profiles in A2V are very similar to those in WT with four β signals of 20% at residues 3–5, 30% at residues 10–12, and 50% at CHC and residues 31–36, and three turn signals of 50–70% at positions H6-G9, H13-Q15, D23-G29, and G37-G38 (Figure 2a and c). The double A2V mutation enhances the α -helix content of H6-Q15 and D23-G29 from (5, 15%) in WT to (10, 30%) in A2V (Figure 2b). The residues L17-F20 and G33-V36 have maximum β -strand values of 75% in MIX vs 50% in WT and A2V, and the β content of residues V12-H13 decrease from 38 to 20% in MIX to 28–12% in WT and 16–6% in A2V. Upon single A2V mutation and compared to WT, the α -helix propensity shifts from 5 to 17% at E3-D7 and from 20 to 10% at L17-G38, the turn character of D23-G29 and L17-F19 is reduced by 10%, and there is little change in the per-residue coil content (Figure 2d).

Intra- and Intermolecular SC–SC Contacts. The intramolecular SC–SC maps are shown in Figure 3. In WT, the contacts with probabilities of >30% are formed between L17 and L34 (39%), V18 and M35 (33%), F19 and L34 (32%), and F20 and M35 (32%). These contacts are observed with similar probabilities in A2V and higher probabilities in MIX: L17-L34 (40, 61%), V18-M35 (31, 45%), F19-L34 (32, 51%), and F20-M35 (30, 47%). In all systems, there are weak contacts between F4-Y10 (7%) and F4-F19 (11%) and long-range intramolecular salt bridges have low probabilities: R5-E11 (16%), E11-K16 (15%), E22-K28 (11%) and D23-K28 (13%). Compared to WT and A2V, MIX displays additional contacts in Nter (E3-V12:18%, R5-V12:20%) and between Nter and CHC (V12-V18:29%).

The intermolecular SC–SC maps in Figure 3 show that the most populated CHC–CHC contacts in WT have probabilities of 12% between L17 and F19, F19 and F20, and F19 and F19. These values are similar in MIX, but lower in A2V and vary from 3 to 6%. The Cter–Cter shows more interactions between the residues I31, I32, L34 and M35 in A2V than in WT and MIX, with maximal probabilities of 12% in A2V and WT and 10% in MIX. The CHC–Cter shows many contacts between the residues L17, F19 and F20 and the residues I32, L34 and V36 with probabilities of 9–11% in WT and A2V, but only two contacts with probabilities of 9% between L17 and I32, and F19 and L34 in MIX. The Nter–CHC shows contacts between Y10 and F19 (11%), Y10 and L17 (7%), and V12 and L17 (7%) in A2V, and these values are lower in WT and MIX (Y10-F19:2.5%, Y10-L17:4%, V12-L17:4%). A2V has more Nter–Nter contacts with probabilities of 3–6% than MIX and WT.

Single-Molecule States. To identify other differences between the variants, we first analyzed their FELs at the single-molecule state. We recall that a single-molecule state is a state of a single-chain in the presence of another chain. The FELs along the intramolecular $Q_{\text{Nter-CHC}}$ and $Q_{\text{Cter-CHC}}$ variables are shown in Figure 4. The k-means clustering analysis reveals eight

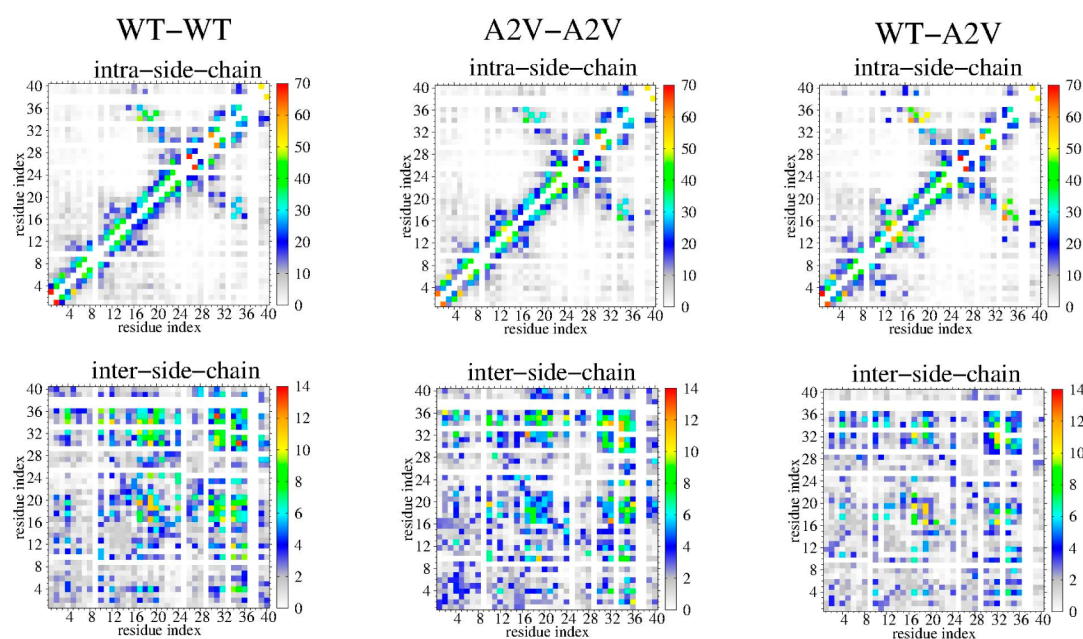


Figure 3. Probability of forming intramolecular (above) and intermolecular (below) side-chain side-chain contacts in the WT (left), A2V (middle), and MIX (right) dimers. Shown are results obtained from 50–400 ns of the REMD trajectory at 315 K. In the intra- and intermolecular contact maps of the MIX, the upper and lower diagonal elements are the results of the WT and A2V chains, respectively.

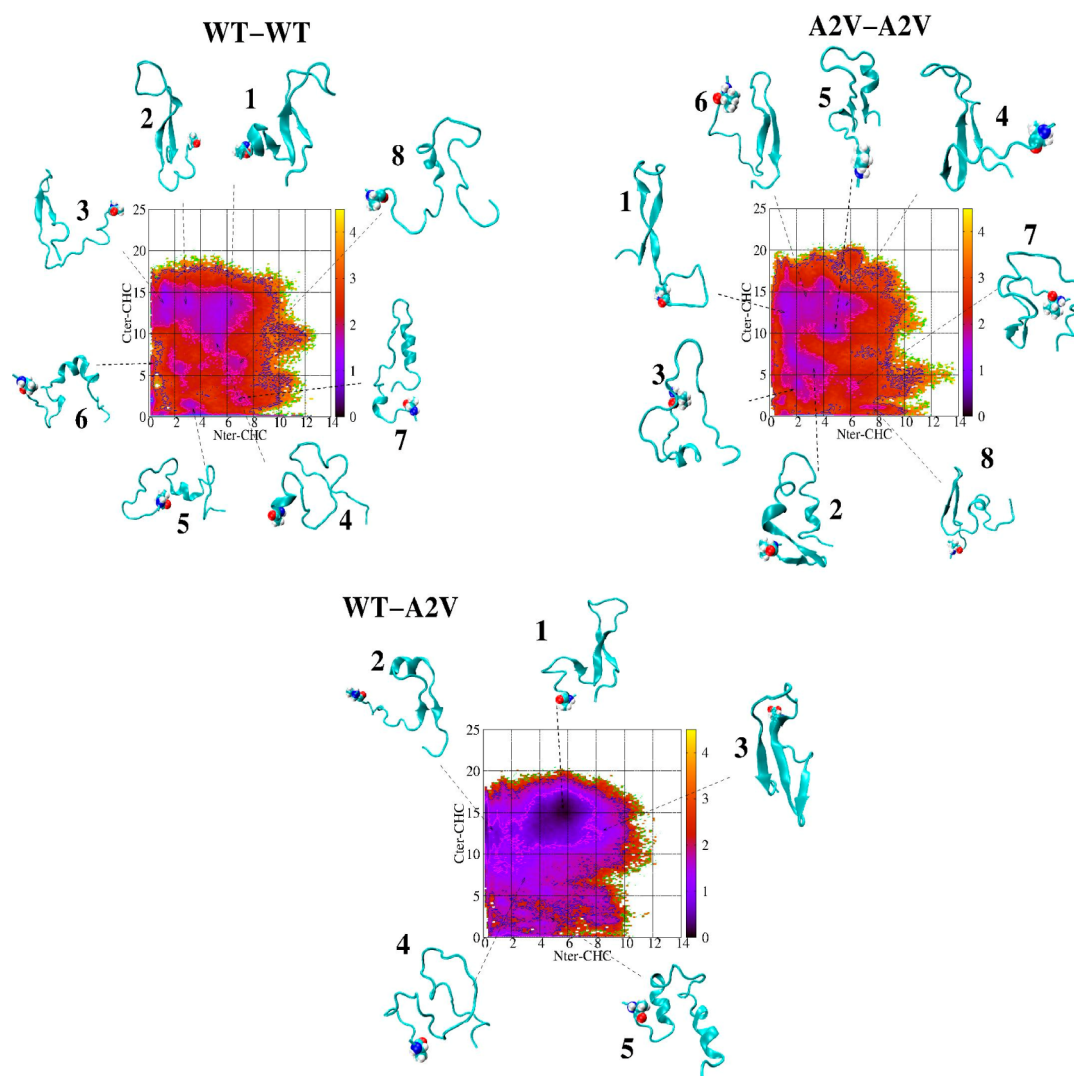


Figure 4. Free energy landscape (in kcal/mol) of the single-molecule state as a function of the two coordinates $Q_{\text{Nter-CHC}}$ and $Q_{\text{Cter-CHC}}$ (see text for the definition). Shown are the representative structures at the cluster centers. The second residue is shown with an all-atom representation.

free energy minima denoted as Ss_i ($i = 1-8$) for WT and A2V, and five free energy minima for WT-A2V. Structures closest to the center of each minimum are shown in Figure 4. Using all structures of each state, the Ss states are described in Table 2 by their Boltzmann populations (P), the β -strand and α -helix populations of the Nter, CHC and Cter, and the mean number of intramolecular SC-SC, Nter-CHC, and Cter-CHC contacts. The number of intra Nter-Cter contacts is not given since it varies between 1 and 3.

In WT, the Ss_1 , Ss_2 and Ss_3 states, representing 43% the ensemble, have a probability of 45–71% to form a β -hairpin at residues K16-F20 and I32-V36 (Ss_1) or at L17-A21 and I31-V36 (Ss_2 and Ss_3) and a probability of 35% to form a three-stranded β -sheet spanning residues 11–13, 16–20 and 32–36. Ss_4 is essentially turn/coil, although it has a probability of 48% and 26% to form β -strands at CHC and Cter. These four states have 10–15 CHC-Cter and 2–6 Nter-CHC contacts. In contrast, the four Ss_5 – Ss_8 states, representing 42% of the ensemble and displaying 1 (Ss_5 and Ss_6) to 7 CHC-Cter contacts and 2–7 Nter-CHC contacts, are mainly coil/turn with transient helices at CHC and Cter (in Ss_5 , probabilities of 20 and 32%), Cter (in Ss_6) or at residues 14–18 (in Ss_8).

In A2V, Ss_1 and Ss_6 with a total population P of 30% are described by structures with few Nter-CHC ($Q = 2$ or 3) and many Cter-CHC ($Q = 12$ or 16) contacts and a β -hairpin probability of 60% formed by K16-A21 and I31-V36 (Ss_1) or V18-D23 and I31-M35 (Ss_6). Ss_4 with $P = 13\%$ displays many CHC-Cter contacts ($Q = 10-16$) and a three-stranded β -sheet spanning 10–12, 15–19, and 32–36 with a probability of 70%. All these states are similar to Ss_1 , Ss_2 , and Ss_3 of WT. States Ss_2 and Ss_3 , with $P = 17$ and 13% and few CHC-Nter ($Q = 2$ or 3) and CHC-Cter ($Q = 6$ or 2) contacts, are turn/coil with transient and short helices in Nter and Cter. Ss_5 with $P = 12\%$, 5 Nter-CHC and 10 CHC-Cter contacts, is disordered with transient helices and strands throughout the sequence. Finally, Ss_7 (7%) and Ss_8 (6.8%) are coil/turn, with weak CHC-Cter ($Q = 2-5$) and strong Nter-CHC ($Q = 7$) contacts and a probability of 15% to form short helices or strands at CHC and Cter.

In contrast to WT and A2V, the FEL of WT-A2V displays one highly populated minimum. Ss_1 ($P = 32\%$) features strong Nter-CHC ($Q = 6$) and Cter-CHC ($Q = 16$) contacts and a β -hairpin at L17-A21 and I32-V36 with a probability of 71% and a three-stranded β -sheet with a probability of 20%. This β -hairpin state is similar to Ss_2 of WT and Ss_1 of A2V. State Ss_2

Table 2. Single-Molecule States^a

Ss	P	(β,α) _{Nter}	(β,α) _{CHC}	(β,α) _{Cter}	Q _{Nter-CHC}	Q _{Cter-CHC}
1	15.82	16, 5	54, 1	37, 1	6	14
2	14.25	9, 3	60, 1	45, 1	2	15
3	14.00	8, 4	45, 5	36, 7	2	12
4	13.32	15, 4	48, 7	26, 10	6	10
5	11.86	9, 6	9, 20	10, 31	2	1
6	11.21	15, 6	18, 9	9, 19	7	1
7	10.02	9, 7	12, 20	7, 32	3	6
8	9.51	24, 4	27, 17	8, 23	7	6
1	18.26	7, 6	45, 4	36, 5	2	12
2	17.45	13, 7	10, 19	12, 27	2	6
3	12.85	13, 7	11, 19	12, 24	3	2
4	12.79	10, 8	52, 2	38, 2	7	14
5	12.53	10, 9	34, 12	26, 13	5	10
6	12.32	8, 7	62, 2	50, 1	3	16
7	7.04	8, 9	15, 11	13, 17	7	5
8	6.76	13, 7	20, 20	15, 12	7	2
1	31.73	11, 8	61, 1	44, 1	6	16
2	22.86	11, 5	51, 1	40, 2	2	13
3	18.79	15, 7	48, 2	31, 4	7	12
4	14.39	10, 6	27, 4	19, 16	2	8
5	12.24	14, 8	19, 9	10, 28	5	3

^aFor each Ss state, shown are the Boltzmann population in %, the population of (β -strand, α -helix) spanning the Nter, CHC, and Cter regions, and the number of intramolecular SC-SC contacts between Nter and CHC, and between Cter and CHC. WT (upper), A2V (middle), MIX (lower).

($P = 23\%$), stabilized by Cter-CHC contacts ($Q = 13$), also forms a β -hairpin at residues L17-F19 and G33-M35 with a probability of 56%, but Nter is more flexible and makes few contacts with CHC or Cter ($Q = 2$). This state is similar to Ss3 of WT. Ss3 ($P = 19\%$) displays a three-stranded β -sheet (probability of 90%) spanning Y10-V12, Q15-E22 and G33-V36. This state is similar to Ss1 of WT. Finally, Ss4 (14%) and Ss5 (12%) are turn/coil with Ss4 displaying little α -helix and β -strand, and Ss5 having helices at residues S8-K16 and K28-V36 with probabilities of 9 and 29%.

Dimer States. Using the product basis of the inter- and intramolecular states (see ref 28 for details), we obtain 320 and 332 dimer states for WT and A2V, and 144 for WT-A2V. Figure 5 shows the representative structures of the first 10 states labeled as Si and covering 22% of the WT and A2V ensemble and 32% of the WT-A2V ensemble.

For the WT dimer, S1 ($P = 2.9\%$) has one β -rich chain forming a β -hairpin (residues L17-F19 and I32-M35) orientated almost perpendicularly to the second α -rich chain (helices at residues G25-G29 and I32-L34). The states S2, S4, S5, and S6 covering 9.3% of the ensemble have high helical contents and result from different single-molecule states. For instance, S2 is characterized by two Ss7 states, while S6 = (Ss5, Ss7). S7 ($P = 1.9\%$) has a eight-stranded β -sheet with the first chain forming a 3-stranded β -sheet spanning residues Y10-H13, L17-F20, and I31-V36, and the second chain forming strands at residues A2-R5, Y10-H13, L17-F19, V24-G25 and I32-M35. S7 has an interchain parallel β -sheet between residues I31-V36 and I32-M35. The S3, S9 and S10 states ($P = 5.8\%$), formed by different β -rich single-molecular states, S3 = (Ss1, Ss3) and S9 = (Ss1, Ss2), display four-stranded (S3, S9) or five-stranded (S10) β -sheets stabilized by interpeptide CHC-Cter contacts. They all feature two intramolecular β -hairpins.

However, there is an interchain antiparallel β -sheet between K16-E22 and A30-L34 in S3, while there is an interchain parallel β -sheet between L17-A21 and M35-V36 in S9, and between L17-A21 and I32-V36 in S10. Finally, the random coil S8 = (Ss6, Ss6) state is stabilized by interpeptide Nter-CHC contacts.

For the A2V states, S1 (3.6%), lacking substantial intramolecular Nter-CHC and Cter-CHC contacts, is essentially disordered, but forms a three-stranded antiparallel β -sheet spanning residues D1-F4 and K16-F20 in one chain and G33-V36 in the second chain. The S8 and S9 states, with a population of 3.5%, have high alpha propensities and are characterized by interchain helical interfaces spanned by residues E11-F20 and N27-G38 in one chain and residues N27-G37 in the second chain (S8), and residues H13-E22 and G29-G38 (S9). The S3, S5, and S7 states with a total population of 6.7% share the same global topology: one chain with a β -hairpin spanning CHC and Cter with no preferred interaction sites with the second chain essentially turn/coil and little alpha and beta characters. Finally, S2 and S6 with a population of 4.7% display two β -hairpins, and S4 and S10 with a population of 4.4% display one β -hairpin and one three-stranded β -sheet. All these states display however different intramolecular conformations and interfaces. S2, characterized by (Ss6, Ss6) and two hairpins, has an interpeptide parallel β -sheet between the two CHCs, namely, residues L17-A21. S6 = (Ss1, Ss6) has the two hairpins almost perpendicular and an interchain parallel β -sheet between I31-V36 and K16-E22. S4 = (Ss1, Ss2) displays an interchain parallel β -sheet between the hairpin and the 3-stranded β -sheet, namely, residues K16-E22 and I31-V36, while in S10 = (Ss4, Ss8) the hairpin is almost antiparallel to the 3-stranded β -sheet and there is no interchain β -sheet.

For the WT-A2V dimer, S1 = (Ss3, Ss4) of population 4.7% is formed by one chain with a 3-stranded β -sheet interacting with the second random coil chain. Interestingly, while S3 has a complex topology with interpeptide antiparallel β -sheets between residues 10-12 and 1-4 and between residues 30-32 and 12-14, the remaining eight states (S2, S4, S5, S6, S7, S8, S9, and S10) with a total population of 24.9% consist of the Ss1 and Ss3 conformations and display one chain adopting a three-stranded β -sheet spanning Nter, CHC, and Cter. This chain interacts with the second chain featuring either a β -hairpin at CHC and Cter (S5, S6, S7, S8, and S10) or a three-stranded β -sheet (S2). These states display various orientations of the chains ranging from antiparallel (S7, S8, and S9), parallel (S6), and perpendicular orientations (S2) to less defined interfaces (S5, S4).

To understand the interplay between intra- and intermolecular interactions and the role of Nter, CHC, and Cter, Figure 6 shows the number of intramolecular CHC-Cter contacts, the intermolecular energies of the peptides and between the Nter-CHC and Cter-CHC regions. Here we use the first 20 states, representing 36% of the WT and A2V ensemble and 52% of the MIX ensemble. On average, the first 20 states of A2V-WT have much higher intramolecular CHC-Cter contacts (Figure 6a), and thus lower intramolecular energies than those in WT and A2V. Compared to WT and A2V, all MIX states, except S3 with -1000 kJ/mol, have much less favorable interpeptide potential energies, varying from -772 in S9 to -206 kJ/mol in S5. The situation changes for A2V compared to WT. On average, the A2V states have much less intramolecular CHC-Cter contacts (except states S2 and S6, Figure 6a) and much favorable

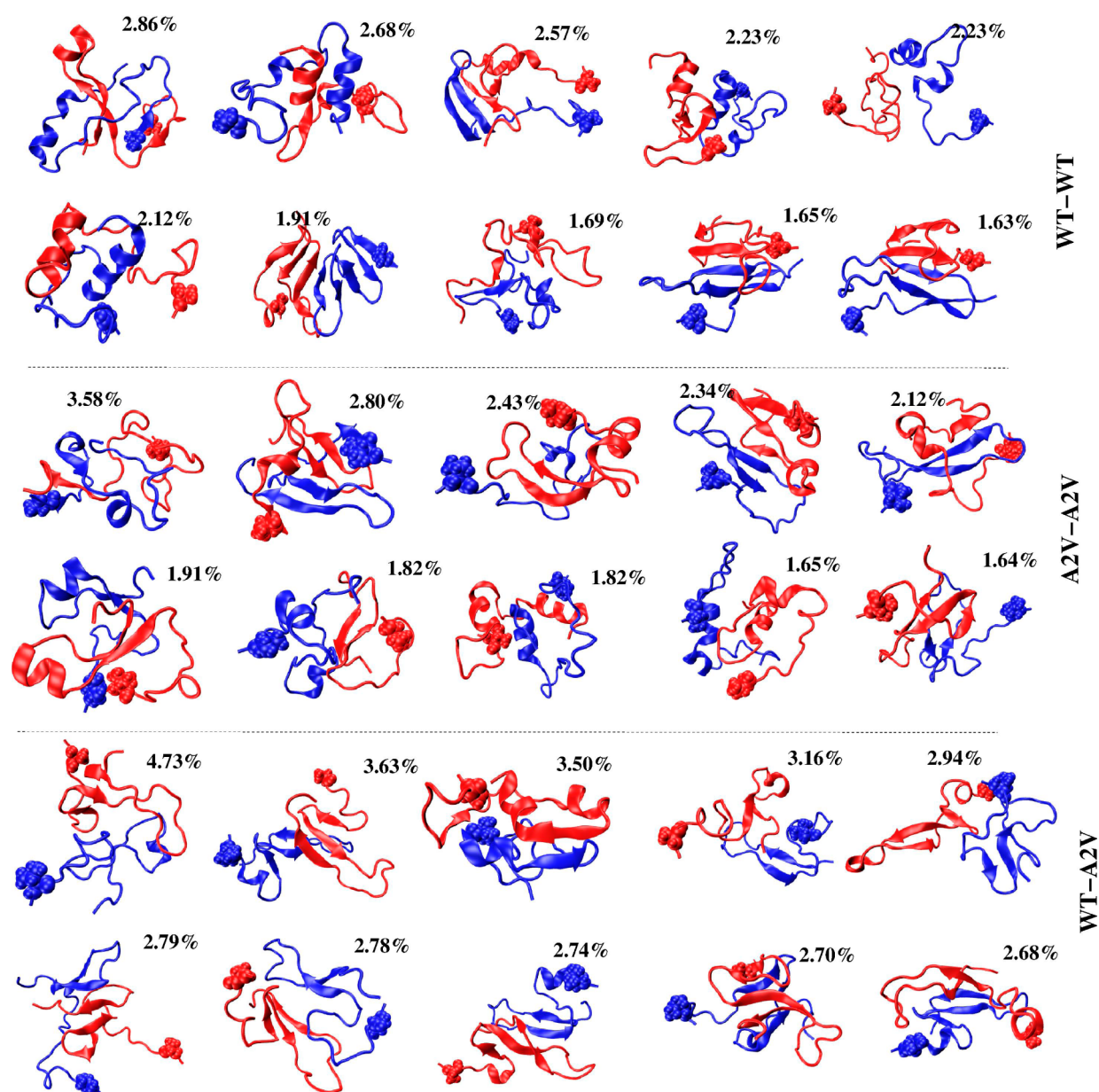


Figure 5. Representative structures of the first 10 overall states of the WT (upper), A2V (middle), and MIX (lower) dimers at 315 K. The population (in %) of each state is also shown. The second residue is shown with an all-atom representation.

interpeptide energies (except states S4, Figure 6b) than the WT states. This is mainly due to more favorable intermolecular CHC-Cter and CHC-Nter contacts (Figure 6c and d) at the expense of less favorable Nter-Nter contacts.

Finally, Figure 7 shows, for the first 100 states of each system, the population of conformations with both chains in α -helical conformations. These 100 states represent more than 95% of the conformational ensemble. We clearly see that the WT and A2V peptides feature many all- α topologies while MIX is almost devoid of them.

Relative to WT, the A2V mutation enhances aggregation kinetics and neurotoxicity and leads to early onset Alzheimer's disease. In contrast, the mixture of WT and A2V peptides enhances the lag phase of fibril formation and protects from AD. For the first time, the conformations of A β 1-40 A2V and WT-A2V dimers have been explored using computer simulations and our findings can be summarized as follows.

First, CD spectra of the A β 1-42 WT, A2V, and MIX oligomeric solutions do not show significant secondary structure differences, with a predominant random coil conformation.¹¹ The exact level of secondary structure variation upon single and double A2V mutation is unknown in A β 1-40, however, the percentage of α -helix content in A β 1-40 WT and its alloforms (A21G, E22G and E22K) as measured by CD does not change much.²³ CD analysis of A β 1-40 WT solutions using different sample preparations indicated (α -helix and β -strand) contents of (10.5 and 38.6%) and (0 and 12%).^{23,24} In agreement with CD, our simulations do not report any change in the averaged secondary structure composition upon double A2V mutation, the (β -strand, α -helix) contents amounting to (18.7, 10%) in WT and (16.8, 11.7%) in A2V. Upon single mutation, the REMD values are (21.7, 6.7%). Differences are better seen at the residue level where the β -strand propensity of residues V12-H13, L17-F20, and G33-V36 have maximum β -strand values of 30, 75, and 75% in MIX vs 11, 50 and 50% in

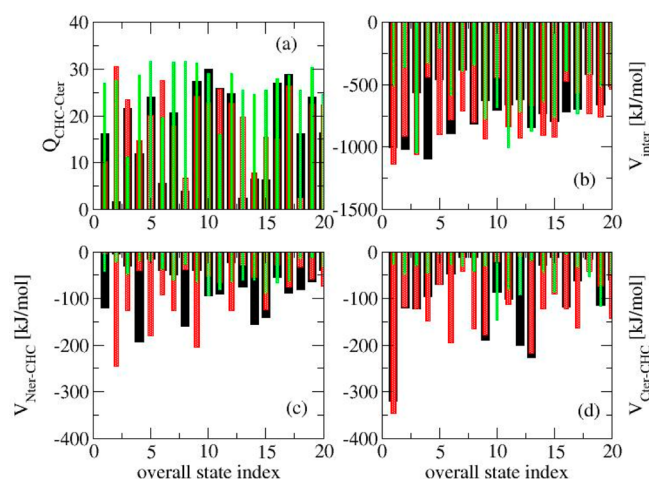


Figure 6. Characterization of the first 20 overall states of the WT (black), A2V (red), and MIX (green) dimers at 315 K. Shown are the total number of the intramolecular contacts between CHC–Cter (a), the total intermolecular potential energy (b), the intermolecular potential energies between Nter–CHC (c), and between Cter–CHC (d).

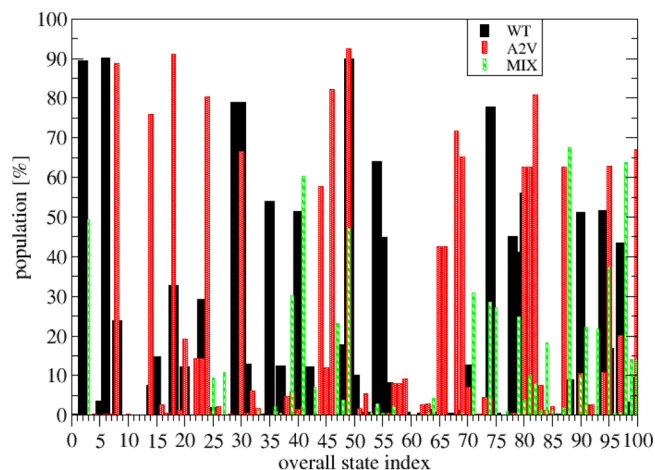


Figure 7. Percentage of all α -topologies for the first 100 states of the dimers for the WT, A2V, and MIX dimers at 315 K. An all- α -topology is defined if both chains have an α -helix alpha with at least four consecutive residues in the α -state, and there are no β -strands. Shown are the results using all conformations of each state.

WT. Also, upon single A2V mutation and compared to WT, the α -helix character shifts from 5 to 17% at E3–D7 and 20 to 10% at L17–G38. Overall, each species shows turns with probabilities $>50\%$ at residues 6–9, 13–15, and 23–29 and β /coil/ α propensities elsewhere. A very similar 2D profile for WT has already been discussed in REMD simulations of A β 1–40 WT monomer at 300 K using various force fields and explicit/implicit solvent models.^{25–27}

Second, WT–A2V significantly reduces the intrinsic disorder of the dimer, but the double A2V mutation does not change this conformational property. Upon single mutation, A2V is found to reduce the number of dimer states by a factor of 2. The intrinsic disorder of proteins has been subject to many simulation studies.^{14,28,29} For instance, Nguyen et al. reported a similar reduction in the conformational ensemble of A β 1–28 monomer upon A2V mutation.¹⁴ Granata et al. showed that the free energy landscape of A β 1–40 monomer at 350 K is inverted

with respect to ordered and folded proteins with the global free energy minimum consisting of highly disordered and extended structures, and many slightly higher free energy conformations with secondary structure arranged in several manners.²⁹ Our work shows that upon A2V single mutation, the number of all- α topologies is significantly reduced. We also show that the MIX dimer states have less favorable interpeptide potential energies. This result is consistent with experimental studies reporting a slower kinetics in MIX due to less stable oligomers.^{7,11} Decrease in interpeptide potential energies of heterozygous dimers may render them more available for degradation.¹ But, reduced toxicity of A2V in heterozygotes may also originate from many sources including different coordination modes with metal ions^{30,31} or lower membrane affinities of small oligomers³² as membrane bound tetramer and trimer A β oligomeric species correlate with toxicity toward cultured neurons.³³

Third, there are significant differences in the intramolecular conformations adopted by the peptide in the three dimers. In WT and A2V, 57, and 54% of the conformations have 8–16 SC–SC CHC–Cter contacts and this population shifts to 70% in MIX. All species populate a very large ensemble of conformations with high coil/turn content and a β -hairpin spanning CHC and Nter, but the hairpin population, registry of H-bonds and SC–SC packing vary with the system. Namely, the β -strands span residues K16–F20 and I32–V36 or L17–A21, and I31–V36 in WT, while they cover K16–A21 and I31–V36 or V18–D23 and I31–M35 in A2V, and L17–A21 and I32–V36 in MIX. This β -hairpin heterogeneity and polymorphism, leading to cross-RMS deviations between 2.4 and 5.6 Å using the residues 16–35, has already been discussed in REMD simulations of A β 1–40, A β 1–28 and A β 1–42 monomers.^{25–27}

The formation and stabilization of the β -hairpin plays an important role in the aggregation of the A β peptides.^{1,31,34} Indeed, when S26 is phosphorylated, residues 23–28 become more rigid and fibrilization is impaired,³⁵ but if D23 and K28 are constrained by a lactam bridge, the aggregation rate is increased by 3 orders of magnitude.³⁶ There is NMR spectroscopy evidence that upon association to the homodimeric Z_{A β 3} protein of 58 residues, the A β 1–40 monomer forms a β -hairpin spanning CHC and the residues 31–36,³⁷ and oligomers of 4–33 A β peptides display antiparallel β -sheets.^{1,38,39} The self-assembly^{32,40} and toxicity³² of A β is also critically dependent on the folding contact between F19 and L34. We find that the probability of this intramolecular contact increases from 32% in A2V and WT to 51% in MIX, thus enhancing the β -hairpin propensity in MIX. Differences in β -hairpin population spanning CHC–CT was also reported by simulation of disulfide bond-locked double mutants (L17C/L34C) of A β 1–40 and A β 17–40 monomers that showed the flexible N-terminal residues help the transfer of entropy to the surrounding solvation shell.⁴¹ Whether this transfer of entropy is observed in our systems will be studied elsewhere.

Another striking difference between the dimer ensembles lies in the association of the two chains and the population of the intramolecular three-stranded β -sheet conformation spanning Nter–CHC–Cter. We find that the population of this folded β -sheet, which ranks in the order: MIX (23%) $>$ WT (15%) and A2V (9%), correlates with the increase in the experimental lag phases for fibril formation: MIX $>$ WT $>$ A2V.⁷ The presence of this transient N-terminal β -strand in A β 1–40 dimers upon single A2V mutation is likely to increase the free energy barrier to convert one molecule to its aggregation-prone state

(consistent with kinetics data⁷) and change the oligomer size distribution (consistent with IM-MS data¹⁰). This additional β -strand may also lead to new oligomer conformations and hence change the overall toxicity. In all three systems, however, a large structural reorganization is still necessary for the structures to fit the amyloid-competent conformations, supporting a traditional polymerization–nucleation mechanism rather than a template-assisted assembly process for amyloid formation.^{1,42}

In summary, the dimerization is critical for the formation of small oligomers, fibril growth, secondary nucleation process and it is a key primary event of the pathogenesis of Alzheimer's disease. Yet, the structural properties of the A β dimer in aqueous solution are largely unknown. Our simulation study provides insights into the complex and long-range effects of the single and double A2V mutation on the A β 1–40 dimers. The results show that the causative and protective effects of A2V mutation in homozygous and heterozygous forms lead to different dimer conformational ensembles with an increase of intramolecular interaction in MIX and of intermolecular interaction in A2V with respect to the wild-type peptide. How the A2V/WT mutation impacts the secondary nucleation rate⁹ remains to be explored. Whether the protective effect of A2T can be rationalized similarly at the structure and thermodynamic molecule and residue levels on the A β 1–40 dimer will be reported elsewhere.

METHODS

Simulation Details. The starting structure for the A2V-WT (MIX) and A2V dimers was taken from our WT dimer (Figure 1 of ref 16), so the three initial structures are identical. As in the WT simulation, the peptides were centered in a truncated octahedron box of 214 nm³ with TIP3P water molecules resulting in a peptide concentration of 15.5 mM. To mimic a 20 mM phosphate buffer used experimentally, we added one H₂PO₄[−] ion and one H₂PO₄^{2−} ion. The peptides at pH 7 have NH₃⁺ and CO₂[−] termini, deprotonated Glu and Asp, protonated Arg and Lys, and neutral His with a protonated N ϵ atom. Each system was neutralized by adding 9 K⁺ ions.

We used the protocol employed for the WT dimer¹⁶ with the GROMACS program.⁴³ The integration time step was 2 fs, electrostatic interactions were calculated using the particle mesh Ewald method and a cutoff of 1.1 nm⁴⁴ and the van der Waals interactions were truncated at 1.2 nm. All simulations were carried out with 60 replicas varying from 300 to 448 K using the temperature method⁴⁵ and the velocity-rescaling thermostat was used for temperature coupling.⁴⁶ Exchanges between neighboring replicas were attempted every 2 ps. The plot of the exchange probabilities as a function of the temperatures shows variations between 21% (310 K) and 25% (340 K), leading to an acceptance ratio of 22% averaged over all temperatures. Each replica ran for 400 ns.

Analysis Details. The secondary structure was calculated using the STRIDE program.⁴⁷ A hydrogen bond (H-bond) was considered formed when the acceptor–donor distance is less than 3.5 Å, and the acceptor–donor–hydrogen angle is less than 30°. A salt-bridge (SB) between two charged side-chains was considered formed if the distance between two specific atoms remains within 4.6 Å.¹⁶ A β -hairpin was defined if there are at least two backbone H-bonds formed between consecutive β -strands, and at least three consecutive residues belonging to the Ramachandran β -strand region in each strand.¹⁶ To capture differences between the three systems, we did not use the common definition for a side-chain–side-chain (SC–SC) contact, namely, a contact between two residues is formed if the minimum distance between any of their heavy SC atoms is <0.45 nm. Rather, we defined the contacts as follows. Let n_{ij} and N_{ij} be the number of heavy atom pairs within a distance <0.45 nm and the number of all heavy atom pairs between residues i and j , and $C_{ij} = n_{ij}/N_{ij}$. Then, the number of contacts between the residues (m_1, m_2) and (n_1, n_2) is defined by $Q = 100 \times \sum_{i=m_1}^{m_2} \sum_{j=n_1}^{n_2} C_{ij}$.

The dimer conformations and their free energy landscapes (FEL) were analyzed using our method that identifies all the structures accurately.⁴⁸ The basis idea is that the intramolecular and intermolecular states are described in terms of combinations of single-molecule and double-molecule states, respectively, and the overall structures of oligomers are the product basis of the intramolecular and intermolecular states.

In the previous analysis of WT dimer, the FEL of a single molecule was constructed using the backbone dihedral angle PCA analysis.¹⁶ Here the FEL was projected onto the two coordinates $Q_{\text{Nter-CHC}}$ and $Q_{\text{Cter-CHC}}$ which are the total number of intramolecular SC–SC contacts between Nter–CHC, and between Cter–CHC, respectively, with Nter spanning residues 1–15, the central hydrophobic core (CHC) spanning residues 16–22 and Cter spanning residues 31–40. Then to obtain the intramolecular states, we carried out clustering analysis using the Hartigan–Wong k-means algorithm as implemented in the R program suite program suite in the R program suite.⁴⁹

To obtain the double-molecule states, we first determined the relative orientations and distances between the two chains, using nine reaction coordinates which are the total numbers of intermolecular SC–SC contacts Q_{x-y} between the regions x and y , where x and y stand for Nter, CHC, and Cter. To obtain the intermolecular states on this nine-dimensional space, we then carried out clustering analysis using the Hartigan–Wong k-means algorithm. Note that, as k-means depends on the initial conditions, for each system, the algorithm was run 2000 times and to obtain the optimal value of the number of clusters, we examined the sum of squares of the observations to their assigned cluster centers and the 30 most popular indices as implemented in NbClust package.¹⁶

AUTHOR INFORMATION

Corresponding Author

*E-mail: philippe.derreumaux@ibpc.fr. Tel: 33 1 58 41 51 72.

Author Contributions

All authors performed simulations and analysis. P.H. Nguyen and P. Derreumaux wrote the manuscript.

Funding

This work was supported by grants from the GRAL ANR SIMI 12-BS07-0017-01. We also acknowledge support from “DYNAMO” ANR-11-LABX-0011, computer time from the IDRIS, CINES, and TGCC centers (Grant x2016077604), and funding from the European Research Council under the European Community's Seventh Framework Program (FP7/2007–2013), Grant Agreement No. 258748.

Notes

The authors declare no competing financial interest.

REFERENCES

- (1) Nastica-Labouze, J., Nguyen, P. H., Sterpone, F., Berthoumieu, O., Buchete, N. V., Coté, S., De Simone, A., Doig, A. J., Faller, P., Garcia, A., et al. (2015) Amyloid beta Protein and Alzheimer's Disease: When Computer Simulations Complement Experimental Studies. *Chem. Rev.* 115, 3518–3563.
- (2) Jin, M., Shepardson, N., Yang, T., Chen, G., Walsh, D., and Selkoe, D. J. (2011) Soluble Amyloid β -protein Dimers Isolated from Alzheimer Cortex directly Induce Tau Hyperphosphorylation and Neuritic Degeneration. *Proc. Natl. Acad. Sci. U. S. A.* 108, 5819–5824.
- (3) Müller-Schiffmann, A., Herring, A., Abdel-Hafiz, L., Chepkova, A. N., Schäble, S., Wedel, D., Horn, A. H., Sticht, H., de Souza Silva, M. A., Gottmann, K., et al. (2016) Amyloid- β dimers in the absence of plaque pathology impair learning and synaptic plasticity. *Brain* 139, 509–525.
- (4) Berthoumieu, O., Nguyen, P. H., Castillo-Frias, M. P., Ferre, S., Tarus, B., Nastica-Labouze, J., Noël, S., Saurel, O., Rampon, C., Doig, A. J., Derreumaux, P., et al. (2015) Combined experimental and simulation studies suggest a revised mode of action of the anti-Alzheimer disease drug NQTrp. *Chem. - Eur. J.* 21, 12657–12666.

- (5) Zhang, T., Zhang, J., Derreumaux, P., and Mu, Y. (2013) Molecular Mechanism of the Inhibition of EGCG on the Alzheimer $A\beta(1-42)$ Dimer. *J. Phys. Chem. B* 117, 3993–4002.
- (6) Doig, A. J., and Derreumaux, P. (2015) Inhibition of Protein Aggregation and Amyloid Formation by Small Molecules. *Curr. Opin. Struct. Biol.* 30, 50–56.
- (7) Di Fede, G., Catania, M., Morbin, M., Rossi, G., Suardi, S., Mazzoleni, G., Merlin, M., Giovagnoli, A. R., Prioni, S., Erbetta, A., et al. (2009) A Recessive Mutation in the APP Gene with Dominant-Negative Effect on Amyloidogenesis. *Science* 323, 1473–1477.
- (8) Cohen, S. I., Linse, S., Luheshi, L. M., Hellstrand, E., White, D. A., Rajah, L., Otzen, D. E., Vendruscolo, M., Dobson, C. M., and Knowles, T. P. (2013) Proliferation of amyloid- β 42 aggregates occurs through a secondary nucleation mechanism. *Proc. Natl. Acad. Sci. U. S. A.* 110, 9758–9763.
- (9) Meisl, G., Yang, X., Frohm, B., Knowles, T. P., and Linse, S. (2016) Quantitative analysis of intrinsic and extrinsic factors in the aggregation mechanism of Alzheimer-associated $A\beta$ -peptide. *Sci. Rep.* 6, 18728.
- (10) Zheng, X., Liu, D., Roychaudhuri, R., Teplow, D. B., and Bowers, M. T. (2015) Amyloid β -Protein Assembly: Differential Effects of the Protective A2T Mutation and Recessive A2V Familial Alzheimer's Disease Mutation. *ACS Chem. Neurosci.* 6, 1732–40.
- (11) Messa, M., Colombo, L., del Favero, E., Cantù, L., Stoilova, T., Cagnotto, A., Rossi, A., Morbin, M., Di Fede, G., Tagliavini, F., et al. (2014) The peculiar role of the A2V mutation in amyloid- β ($A\beta$) 1–42 molecular assembly. *J. Biol. Chem.* 289, 24143–52.
- (12) Lindorff-Larsen, K., Piana, S., Dror, R. O., and Shaw, D. E. (2011) How Fast Proteins Fold. *Science* 334, 517–520.
- (13) Zhang, T., Nguyen, P. H., Nasica-Labouze, J., Mu, Y., and Derreumaux, P. (2015) Folding Atomistic Proteins in Explicit Solvent Using Simulated Tempering. *J. Phys. Chem. B* 119, 6941–6951.
- (14) Nguyen, P. H., Tarus, B., and Derreumaux, P. (2014) Familial Alzheimer A2V Mutation Reduces the Intrinsic Disorder and Completely Changes the Free Energy Landscape of the Ab1–28 Monomer. *J. Phys. Chem. B* 118, 501–510.
- (15) Tarus, B., Nguyen, P. H., Berthoumieu, O., Faller, P., Doig, A. J., and Derreumaux, P. (2015) Molecular Structure of the NQTrp Inhibitor with the Alzheimer Abeta1–28 Monomer. *Eur. J. Med. Chem.* 91, 43–50.
- (16) Tarus, B., Tran, T. T., Nasica-Labouze, J., Sterpone, F., Nguyen, P. H., and Derreumaux, P. (2015) Structures of the Alzheimer's Wild-Type $A\beta$ 1–40 Dimer from Atomistic Simulations. *J. Phys. Chem. B* 119, 10478–87.
- (17) Urbanc, B., Betnel, M., Cruz, L., Bitan, G., and Teplow, D. B. (2010) Elucidation of Amyloid β -protein Oligomerization Mechanisms: Discrete Molecular Dynamics Study. *J. Am. Chem. Soc.* 132, 4266–4280.
- (18) Barz, B., and Urbanc, B. (2012) Dimer Formation Enhances Structural Differences between Amyloid β -protein (1–40) and (1–42): an Explicit-solvent Molecular Dynamics Study. *PLoS One* 7, e34345.
- (19) Viet, M. H., Nguyen, P. H., Ngo, S. T., Li, M. S., and Derreumaux, P. (2013) Effect of the Tottori Familial Disease Mutation (D7N) on the Monomers and Dimers of $A\beta$ 40 and $A\beta$ 42. *ACS Chem. Neurosci.* 4, 1446–1457.
- (20) Nguyen, P., and Derreumaux, P. (2014) Understanding amyloid fibril nucleation and $a\beta$ oligomer/drug interactions from computer simulations. *Acc. Chem. Res.* 47, 603–11.
- (21) Sterpone, F., Melchionna, S., Tuffery, P., Pasquali, S., Mousseau, N., Cragnolini, T., Chebaro, Y., St-Pierre, J., Kalimeri, M., Barducci, A., et al. (2014) The OPEP Protein Model: From Single Molecules, Amyloid Formation, Crowding and Hydrodynamics to DNA/RNA Systems. *Chem. Soc. Rev.* 43, 4871–4893.
- (22) Das, P., Murray, B., and Belfort, G. (2015) Alzheimer's protective A2T mutation changes the conformational landscape of the $A\beta$ 1–42 monomer differently than does the A2V mutation. *Biophys. J.* 108, 738–47.
- (23) Kirkitadze, M. D., Condrion, M. M., and Teplow, D. B. (2001) Identification and Characterization of Key Kinetic Intermediates in Amyloid β -protein Fibrillogenesis. *J. Mol. Biol.* 312, 1103–1119.
- (24) Ono, K., Condrion, M. M., and Teplow, D. B. (2009) Structure-neurotoxicity Relationships of Amyloid β -protein Oligomers. *Proc. Natl. Acad. Sci. U. S. A.* 106, 14745–14750.
- (25) Rosenman, D. J., Connors, C. R., Chen, W., Wang, C., and Garcia, A. E. (2013) Abeta Monomers transiently Sample Oligomer and Fibril-like Configurations: Ensemble Characterization using a Combined MD/NMR approach. *J. Mol. Biol.* 425, 3338–3359.
- (26) Rosenman, D. J., Wang, C., and Garcia, A. E. (2016) Characterization of $A\beta$ Monomers through the Convergence of Ensemble Properties among Simulations with Multiple Force Fields. *J. Phys. Chem. B* 120, 259–277.
- (27) Côté, S., Derreumaux, P., and Mousseau, N. (2011) Distinct Morphologies for Amyloid Beta Protein Monomer: $A\beta$ 1–40, $A\beta$ 1–42, and $A\beta$ 1–40(D23N). *J. Chem. Theory Comput.* 7, 2584–2592.
- (28) De Simone, A., Kitchen, C., Kwan, A. H., Sunde, M., Dobson, C. M., and Frenkel, D. (2012) Intrinsic disorder modulates protein self-assembly and aggregation. *Proc. Natl. Acad. Sci. U. S. A.* 109, 6951–6956.
- (29) Granata, D., Baftizadeh, F., Habchi, J., Galvagnion, C., De Simone, A., Camilloni, C., Laio, A., and Vendruscolo, M. (2015) The inverted free energy landscape of an intrinsically disordered peptide by simulations and experiments. *Sci. Rep.* 5, 15449.
- (30) Dorlet, P., Gambarelli, S., Faller, P., and Hureau, C. (2009) Deprotonation of the Asp1-Ala2 peptide bond induces modification of the dynamic copper(II) environment in the amyloid-beta peptide near physiological pH. *Angew. Chem., Int. Ed.* 48, 9273–9276.
- (31) Xu, L., Shan, S., Chen, Y., Wang, X., Nussinov, R., and Ma, B. (2015) Coupling of Zinc-Binding and Secondary Structure in Nonfibrillar $A\beta$ 40 Peptide Oligomerization. *J. Chem. Inf. Model.* 55, 1218–1230.
- (32) Das, A. K., Rawat, A., Bhowmik, D., Pandit, R., Huster, D., and Maiti, S. (2015) An Early Folding Contact between Phe19 and Leu34 is Critical for Amyloid- β Oligomer Toxicity. *ACS Chem. Neurosci.* 6, 1290–1295.
- (33) Munter, L. M. (2016) How many amyloid- β peptides can a neuron bind before it dies? *J. Neurochem.* 136, 437–439.
- (34) Fu, Z., Aucoin, D., Davis, J., Van Nostrand, W. E., and Smith, S. O. (2015) Mechanism of Nucleated Conformational Conversion of $A\beta$ 42. *Biochemistry* 54, 4197–207.
- (35) Rezaei-Ghaleh, N., Amininasab, M., Giller, K., Kumar, S., Stündl, A., Schneider, A., Becker, S., Walter, J., and Zweckstetter, M. (2014) Turn plasticity distinguishes different modes of amyloid- β aggregation. *J. Am. Chem. Soc.* 136, 4913–4919.
- (36) Sciarretta, K. L., Gordon, D. J., Petkova, A. T., Tycko, R., and Meredith, S. C. (2005) Abeta40-Lactam(D23/K28) models a conformation highly favorable for nucleation of amyloid. *Biochemistry* 44, 6003–6014.
- (37) Hoyer, W., Grönwall, C., Jonsson, A., Ståhl, S., and Härd, T. (2008) Stabilization of a β -Hairpin in Monomeric Alzheimer's Amyloid- β Peptide Inhibits Amyloid Formation. *Proc. Natl. Acad. Sci. U. S. A.* 105, 5099–5104.
- (38) Ahmed, M., Davis, J., Aucoin, D., Sato, T., Ahuja, S., Aimoto, S., Elliott, J. I., Van Nostrand, W. E., and Smith, S. O. (2010) Structural conversion of neurotoxic amyloid-beta(1–42) oligomers to fibrils. *Nat. Struct. Mol. Biol.* 17, 561–567.
- (39) Tay, W. M., Huang, D., Rosenberry, T. L., and Paravastu, A. K. (2013) The Alzheimer's amyloid- β (1–42) peptide forms off-pathway oligomers and fibrils that are distinguished structurally by intermolecular organization. *J. Mol. Biol.* 425, 2494–2508.
- (40) Potapov, A., Yau, W. M., Ghirlando, R., Thurber, K. R., and Tycko, R. (2015) Successive Stages of Amyloid- β Self-Assembly Characterized by Solid-State Nuclear Magnetic Resonance with Dynamic Nuclear Polarization. *J. Am. Chem. Soc.* 137, 8294–307.
- (41) Xu, L., Nussinov, R., and Ma, B. (2016) Allosteric stabilization of the amyloid- β peptide hairpin by the fluctuating N-terminal. *Chem. Commun. (Cambridge, U. K.)* 52, 1733–1736.

- (42) Li, M. S., Klimov, D. K., Straub, J. E., and Thirumalai, D. (2008) Probing the mechanisms of fibril formation using lattice models. *J. Chem. Phys.* *129*, 175101.
- (43) Van der Spoel, D., Lindahl, E., Hess, B., Groenhof, G., Mark, A. E., and Berendsen, H. J. (2005) GROMACS: Fast, Flexible, and Free. *J. Comput. Chem.* *26*, 1701–1718.
- (44) Essmann, U., Perera, L., Berkowitz, M. L., Darden, T., Lee, H., and Pedersen, L. G. (1995) A Smooth Particle Mesh Ewald Method. *J. Chem. Phys.* *103*, 8577–8593.
- (45) Patriksson, A., and van der Spoel, D. A. (2008) Temperature Predictor for Parallel Tempering Simulations. *Phys. Chem. Chem. Phys.* *10*, 2073–2077.
- (46) Bussi, G., Donadio, D., and Parrinello, M. (2007) Canonical Sampling through Velocity Rescaling. *J. Chem. Phys.* *126*, 014101.
- (47) Frishman, D., and Argos, P. (1995) Knowledge-based Protein Secondary Structure Assignment. *Proteins: Struct., Funct., Genet.* *23*, 566–579.
- (48) Nguyen, P. H., Li, M. S., and Derreumaux, P. (2014) Amyloid Oligomer Structure Characterization from Simulations: a General Method. *J. Chem. Phys.* *140*, 094105.
- (49) Hartigan, J. A., and Wong, M. A. (1979) A k-Means Clustering Algorithm. *Appl. Statist* *28*, 100–108.